Journal of Physics: Conference Series

OPEN ACCESS

Analytical modelling of soil effects on electromagnetic induction sensor for humanitarian demining

To cite this article: D Vasić *et al* 2013 *J. Phys.: Conf. Ser.* **450** 012052

View the article online for updates and enhancements.

You may also like

- Characterization and reduction of background noise for the detection of plastic anti-personnel landmine in mineralized soil
J. Ge, W. Luo, H. Dong et al.
- Study on the variation law of shock wave on the surface of landmine shell under touchdown explosion
Jiahui Chen and Deren Kong
- Active induction balance method for metal detector sensing head utilizing transmitter-bucking and dual current source
D Ambruš, D Vasi and V Bilas

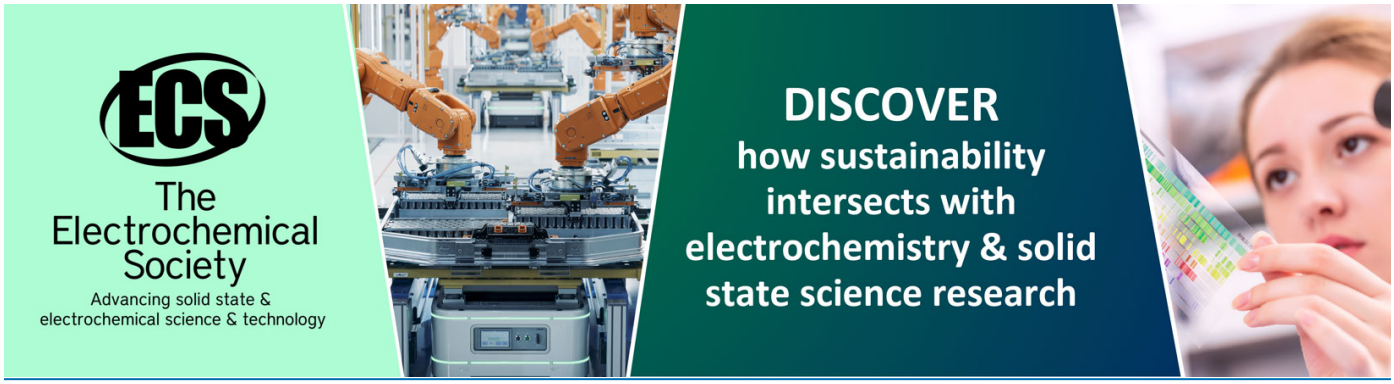

This content was downloaded from IP address 3.142.114.91 on 15/05/2024 at 23:35

Analytical modelling of soil effects on electromagnetic induction sensor for humanitarian demining

D Vasić, D Ambruš and V Bilas

University of Zagreb, Faculty of Electrical Engineering and Computing
FER-ZESOI, Unska 3, HR-10000 Zagreb, Croatia

E-mail: darko.vasic@fer.hr

Abstract. Accurate compensation of the soil effect is essential for a new generation of sensitive classification-based electromagnetic induction landmine detectors. We present an analytical model for evaluation of the soil effect suitable for straightforward numerical implementation. The modelled soil consists of arbitrary number of conductive and magnetic layers. The solution region is truncated leading to the solution in form of a series rather than infinite integrals. Frequency-dependent permeability is inherent to the model, and time domain analysis can be made using DFT. In order to illustrate the model usage, we evaluate performances of three metal detector designs.

1. Introduction

Electromagnetic induction (EMI) sensors in the form of metal detectors for humanitarian demining are the most important devices for close-in landmine detection well suited to the field applications due to their robustness and sensitivity achievable by a skilled operator [1]. The research of EMI sensors for landmine detection is directed towards reducing the number of false alarms and increasing the speed either by combining the metal detector with other established methods such as ground penetrating radar (GPR) or by employing more advanced mine detection EMI techniques based on mine or clutter classification of metallic objects according to their material, shape and dimensions [1], [2].

Degradation of metal detector performances in certain soil types has been known since World War II, but the research on the soil effects was somewhat neglected by the mine detection community until recently [3]. The studies of the soil effects employed models of homogenous half-space soil based on the infinite integral formulation of the soil response, usually followed by the approximations for low or negligible electrical conductivity and magnetic permeability [3], [4]. Although useful for understanding of the soil effects on metal detectors in general, e.g. dominant effect of frequency-dependent magnetic permeability, such models may be insufficient for new generation of metal detectors based on the classification algorithms that require accurate soil effect compensation [2].

In this paper we present an analytical frequency-domain model for calculation of the magnetic field and induced voltage for a sensor head located above arbitrary number of conductive and magnetic soil layers. The solution region is truncated leading to the solution in form of a series rather than infinite integrals [5], [6]. This allows easier and faster implementation and error control [6]. The frequency dependence of permeability is inherent to the model and time domain analysis is possible using DFT. The equations are presented in a form suitable for straightforward stable numerical implementation. Using the model, we evaluate three typical configurations of metal detectors with respect to ratio of small metallic target response to the soil response [2], [4].


Content from this work may be used under the terms of the Creative Commons Attribution 3.0 licence. Any further distribution of this work must maintain attribution to the author(s) and the title of the work, journal citation and DOI.
Published under licence by IOP Publishing Ltd

2. Analytical model

2.1. Vector magnetic potential and magnetic field

We derived the analytical model of the magnetic potential of a single-turn transmitter coil positioned above a half-space of arbitrary number of conductive and magnetically permeable layers, as depicted in figure 1. In contrast to the usual Dodd and Deeds integral formulation [5], we truncated the solution region and, as a consequence, formulated the solution of the vector magnetic potential equation as a series [6]. The problem domain should be at least ten times larger than the characteristic length of the sensor head: transmitter coil diameter or transmitter-receiver distance, whichever is greater.

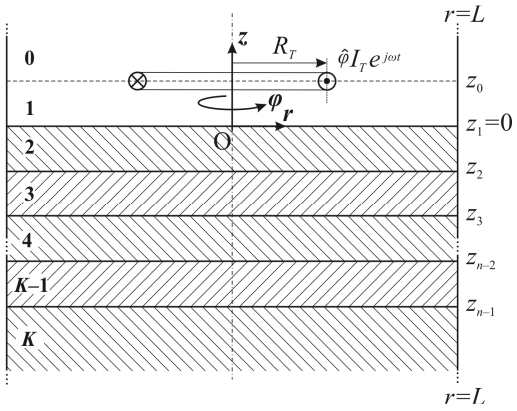

Figure 1. Geometry used for modelling of the soil effects.

The transmitter single-turn coil of radius R_T at height z_0 from the ground is driven by a sinusoidal current i_T of constant amplitude I_T and frequency $\omega = 2\pi f$. The ground is assumed to be composed of $K-1$ linear, isotropic, and homogeneous layers. Electrical conductivity of k-th layer ($k = 2,...K$) is σ_k, its relative magnetic permeability is μ_{rk}, and its thickness is $\Delta z_k = z_{k-1} - z_k$, except that of the K-th layer, where $z_k < z_{k-1} < 0$ as in figure 1. The K-th layer is the region $z < z_{K-1}$ and its thickness is infinite. The problem domain is truncated at $r = L$, whereas it is unbounded in both z directions. In the cylindrical coordinate system, the excitation current has φ component only, and so will the vector magnetic potential **A** too. Taking the axial symmetry into the account and using the quasistatic approximation, the governing equation for the magnetic potential is

$$\frac{\partial^2 A_k(r,z)}{\partial r^2} + \frac{1}{r}\frac{\partial A_k(r,z)}{\partial r} + \frac{\partial^2 A_k(r,z)}{\partial z^2} - \frac{A_k(r,z)}{r^2} - j\omega\mu_0\mu_{rk}\sigma_k A_k(r,z) = 0\,, \tag{1}$$

where A_k is the φ component of **A** in the k-th region. The method of separation of variables reduces (1) into two equations (ordinary differential equation in z and first-order Bessel equation in r).

The magnetic potential for each region must satisfy the homogenous Dirichlet condition

$$A_k(r = L, z) = 0\,. \tag{2}$$

Because of (2), the eigenvalues are discrete and the solution for each region can be written in terms of the series truncated to N elements

$$A_k(r,z) = \sum_{i=1}^{N}\left[C_{k,i}\exp(-\alpha_i z) + D_{k,i}\exp(\alpha_i z)\right]J_1(\alpha_i r), \quad k = 0 \text{ or } k = 1\,, \tag{3}$$

$$A_k(r,z) = \sum_{i=1}^{N}\left[C_{k,i}\exp(-\alpha_{k,i} z) + D_{k,i}\exp(\alpha_{k,i} z)\right]J_1(\alpha_i r), \quad k = 2,\ldots K\,, \tag{4}$$

where $C_{k,i}$ and $D_{k,i}$ are constants to be found out and J_1 is the first-order Bessel function of the first kind. The eigenvalues α_i for regions 0 and 1 (air) are given as solutions of the equation

$$J_1(\alpha_i L) = 0,\ \alpha_1 < \alpha_i < \alpha_N,\ i = 1,\dots N\,. \tag{5}$$

The zeros of the Bessel function can be readily determined using the prepared tables or a numerical root finding algorithm. The eigenvalues for the regions $k = 2,...K$ are

$$\alpha_{k,i} = \sqrt{\alpha_i^2 + j\omega\mu_0\mu_{r,k}\sigma_k}\,, \quad k = 2,\dots K\,. \tag{6}$$

Constants $D_{0,i}$ and $C_{K,i}$ are 0 because of the divergence of the respective exponential functions for $z \to \pm\infty$. The remaining constants have to be calculated from the standard interface conditions for the magnetic field. Using the orthogonal property of the Bessel functions, one can write N systems (for each i) of $2K$ linear equations with $2K$ unknowns $[C_{0,i}\ C_{1,i}\ D_{1,i}\ C_{2,i}\ D_{2,i}\ ...\ C_{K-1,i}\ D_{K-1,i}\ D_{K,i}]^{\mathrm{T}}$. We will report only the potential for $k = 1$, since it is the one required for evaluation of detector performances.

Let $\mathbf{F}_k$ be the characteristic matrix of the k-th region:

$$\mathbf{F}_{k,i} = \begin{bmatrix} 1 & -\dfrac{\mu_{rk}}{\alpha_{k,i}}\tanh\left(-\alpha_{k,i}\Delta z_k\right) \\ -\dfrac{\alpha_{k,i}}{\mu_{rk}}\tanh\left(-\alpha_{k,i}\Delta z_k\right) & 1 \end{bmatrix}, \quad i = 1,\dots N,\ k = 2,\dots K-1\,. \tag{7}$$

It can be shown by solving the linear system that if

$$\mathbf{G}_i = \begin{bmatrix} g_{1,i} \\ g_{2,i} \end{bmatrix} = \begin{bmatrix} 1 & -1/\alpha_i \\ 1 & 1/\alpha_i \end{bmatrix} \left(\prod_{k=2}^{K-1} \mathbf{F}_{k,i} \right) \begin{bmatrix} 1 \\ \alpha_K/\mu_{rK} \end{bmatrix}, \quad i = 1,\dots N\,, \tag{8}$$

then the relation between the constants for the region $k = 1$ is

$$C_{1,i} = \frac{g_{1,i}}{g_{2,i}} D_{1,i}\,, \quad i = 1,\dots N\,. \tag{9}$$

Furthermore, it can be shown that $D_{1,i}$ does not depend on the soil properties and that it is the same as in the case when there is no soil in the vicinity of the coil (coil in the air), i.e.

$$D_{1,i} = \frac{\mu_0 R_T I_T}{L^2} \frac{J_1(\alpha_i R_T)}{\alpha_i J_0^2(\alpha_i L)} \exp(-\alpha_i z_0), \quad i = 1,\dots N\,. \tag{10}$$

Finally, combining (3) with (7)–(10), one can write for the potential for $k = 1$ ($0 \le z \le z_0$)

$$A_1 = A_{1,air} + A_{1,soil} = \sum_{i=1}^{N} D_{1,i} \exp(\alpha_i z) J_1(\alpha_i r) + \sum_{i=1}^{N} \frac{g_{1,i}}{g_{2,i}} D_{1,i} \exp(-\alpha_i z) J_1(\alpha_i r)\,. \tag{11}$$

The magnetic potential is sum of the magnetic potential of the coil in air and the soil response. The only soil-dependent part in (11) is ratio $g_{1,i}/\,g_{2,i}$. Due to the axial symmetry, the magnetic field has only r and z components, and these can be calculated from (11) (calculating $\nabla \times \mathbf{A}$)

$$B_{1,r} = -\frac{\partial A_1}{\partial z} = -\sum_{i=1}^{N} \alpha_i D_{1,i} \exp(\alpha_i z) J_1(\alpha_i r) + \sum_{i=1}^{N} \alpha_i \frac{g_{1,i}}{g_{2,i}} D_{1,i} \exp(-\alpha_i z) J_1(\alpha_i r)\,, \tag{12}$$

$$B_{1,z} = \frac{A_1}{r} + \frac{\partial A_1}{\partial r} = \sum_{i=1}^{N} \alpha_i D_{1,i} \exp(\alpha_i z) J_0(\alpha_i r) + \sum_{i=1}^{N} \alpha_i \frac{g_{1,i}}{g_{2,i}} D_{1,i} \exp(-\alpha_i z) J_0(\alpha_i r)\,. \tag{13}$$

2.2. Induced voltage

Voltage U_R induced in a receiver coil of radius R_R placed at location (r_R, z_R) can be calculated using

$$U_R = j\omega \oint_{C_{RX}} \mathbf{A} \cdot d\vec{l} = j\omega \int_0^{2\pi} A\left(r(\theta), z_R\right) \frac{R_R^2 + R_R r_R \cos(\theta)}{r(\theta)} d\theta, \tag{14}$$

where $r^2(\theta) = R_R^2 + 2R_R r_R \cos(\theta) + r_R^2$. Integral in (14) can easily be calculated using standard numerical integration techniques. The two components of U_R are direct-coupling component, $U_{R,air}$, and soil-related component, $U_{R,soil}$.

2.3. Sensor head sensitivity

A useful concept for analysing and comparing different types of sensor heads is the sensitivity defined for a location in space as

$$S = \frac{\mathbf{H}_T \mathbf{H}_R}{I_T I_R}, \tag{15}$$

where $\mathbf{H}_T$ is the magnetic field produced by the transmitter coil in air energized with current I_T, and $\mathbf{H}_R$ is the magnetic field that the receiver coil in air would produce if it was energized with the current I_R [4], [7]. In the first approximation, if a small and spherical metallic object is introduced in the vicinity of the transmitter-receive pair, the change in the receiver's induced voltage is

$$U_{R,obj} = MS, \tag{16}$$

where M depends only on the object's properties and excitation frequency. The sensitivity defined with (15) does not depend on the metallic object or on the excitation frequency [7].

2.4. Numerical implementation

The discrete eigenvalues allow easier numerical implementation and accuracy control. The convergence of the series is discussed in [6]. The required number of series elements primarily increases with the size of the solution region. For all calculations in this paper, we placed the solution region boundary at $L = 5$ m and we truncated series (11) to $N = 20000$. Using these settings, the numerical accuracy of the magnetic potential was at least 5 significant digits at the regions' boundaries and more than 8 digits otherwise. The model was implemented in MATLAB. It takes about 9 ms to calculate the potential at one point in space for a fixed geometry and $N = 20000$ using Intel Quad CPU and 8 GB of RAM. The execution time increases linearly with N.

3. Results

Using the numerical implementation of the model presented in section 2, we analysed performances of the three typical sensor head designs, schematically depicted in figure 2. The circular sensor head is the most basic design normally used with pulsed excitation in order to avoid excessive direct coupling component in the received voltage. Here, we use it with the harmonic excitation as a standard for comparison against other two types of sensor heads from figure 2. In the OO balanced sensor, transmitter and receiver overlap precisely so that the induced voltage is minimal or preferably zero in air. Finally, the transmitter-bucking configuration employs two transmitter coils with the radii and excitation currents precisely calculated so that the induced voltage is zero. The latter allows easier and more precise control of the minimal induced voltage.

Figure 3 depicts sensitivity isolines in r-z plane ($z < 0$) for all three investigated sensor heads positioned at z = 5 cm above the ground. The circular head sensitivity and the transmitter-bucking head sensitivity are symmetrical around $r = 0$ and they are highest at a given depth along the line. The OO balanced head sensitivity is highest at a given depth along the line $r = 14$ cm that is different from the centre of the coils' overlapping region (at $r = 11.4$ cm). Along these maximum lines, the circular

and OO balanced sensor heads have similar sensitivities because of the same transmitter design. The transmitter-bucking design has the sensitivity smaller for 5 to 10 times compared to the circular head. This means that for the same spherical target, the transmitter-bucking sensor head will produce 5 to 10 times smaller induced voltage depending on the target depth. It should be noted, however, that the transmitter-bucking head has the smallest receiver coil.

Figure 4 depicts the relationship between the sensor head position above the ground (lift-off) and the soil-related component of the induced voltage at the excitation frequency of 100 kHz and for the soil conductivity of 0.01 S/m and relative permeability of 1.01. The inductive balance design (OO balanced and transmitter-bucking heads) significantly reduces the soil effect.

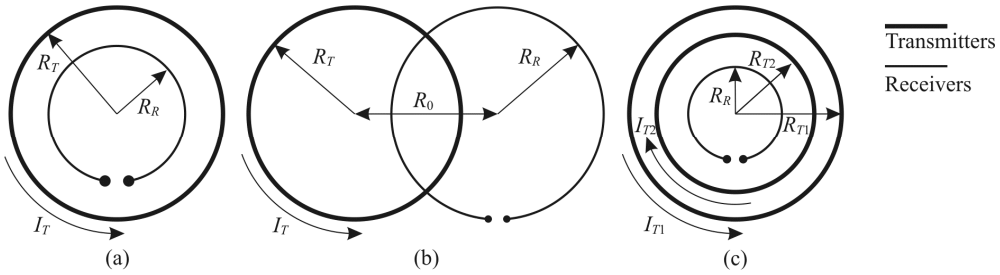

Figure 2. (a) Concentric sensor head (R_T = 15 cm, R_R = 10 cm); **(b)** OO balanced sensor head (R_T = R_R = 15 cm, R_0 = 22.74 cm); **(c)** transmitter-bucking sensor head (R_{T1} = 15 cm, R_{T2} = 6 cm, R_R = 4 cm, I_{T1} = 3I_{T2}).

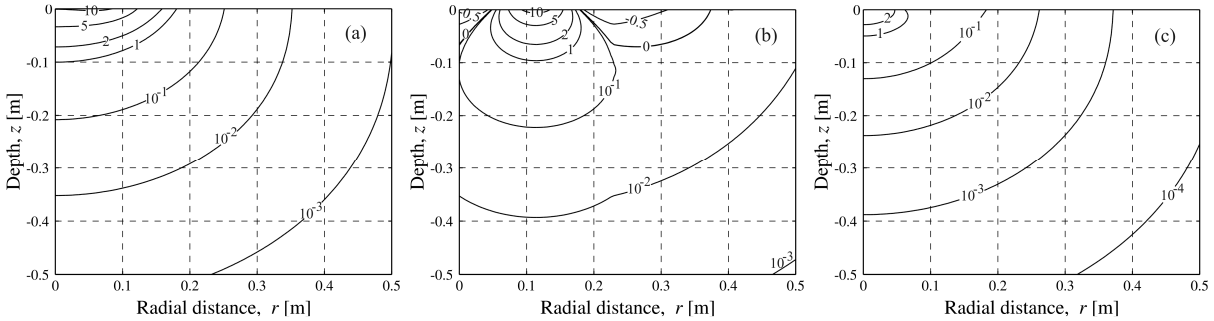

Figure 3. Sensitivity isolines [m^{-2}] for **(a)** circular sensor head, **(b)** OO balanced sensor head, **(c)** transmitter-bucking sensor head. Sensor heads are positioned at z = 5 cm.

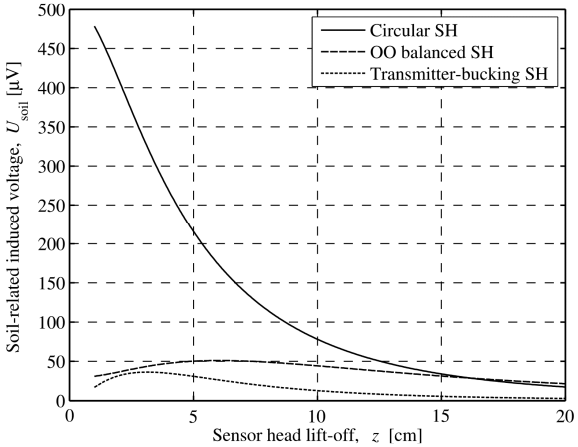

Figure 4. Soil-related (excitation frequency 100 kHz, half-space soil model, σ = 0.1 S/m, μ_r = 1.01) component of the receiver voltage vs. sensor head lift-off.

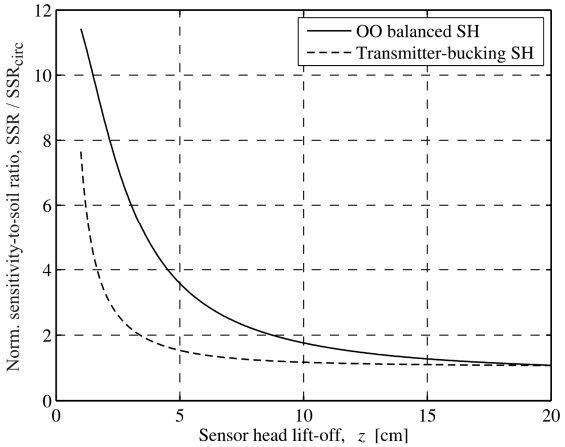

Figure 5. Relationship between lift-off and normalised SSR according to (18) along the lines of the highest sensitivity (constant r). The soil responses are from figure 4.

In order to compare performances of the OO balanced and transmitter-bucking sensor heads in detecting small metallic objects in the presence of soil (σ = 0.01 S/m and μ_r = 1.01), we introduce the sensitivity-to-soil signal ratio (*SSR*)

$$SSR = \frac{U_{R,obj}}{U_{R,soil}} = \frac{MS}{U_{R,soil}}, \tag{17}$$

and to avoid the effect of the metallic object properties, we normalize it with respect to *SSR* of the circular sensor head

$$\frac{SSR}{SSR_{circ}} = \frac{S}{S_{circ}} \frac{U_{R,soil}^{(circ)}}{U_{R,soil}}. \tag{18}$$

The normalized *SSR* vs. lift-off is shown in figure 5. For a given metallic object, the ratio of the target and soil components of the induced voltage for OO balanced and transmitter-bucking sensor heads is larger (up to 10 times) than the ratio for the circular sensor head. The ratio is the largest for the OO balanced sensor, but the transmitter-bucking head has smaller dimensions, easier balancing control and smaller absolute values of the direct coupling and soil-related components of the induced voltage.

4. Conclusions

We presented an analytical model for evaluation of the soil effects on EMI landmine detector in a form suitable for straightforward numerical implementation. The modelled soil consists of arbitrary number of homogeneous, conductive and permeable layers. The solution region is truncated leading to discrete eigenvalues and the solution in form of a series rather than infinite integral. This allows better convergence control and faster numerical implementation. In order to illustrate the usage of the model, we calculated sensitivities of three typical metal detector designs, evaluated the soil effect and the ratio of the metal target signal and soil response. The model is applicable to soil effect correction procedures for new generation of sensitive classification-based EMI landmine detectors. Future work will focus on extending the model to accommodate any orientation and shape of transmitter coils using the second-order vector potential.

Acknowledgement

This research has been partly supported by the Croatian Ministry of Science, Education and Sport through grant agreement 036-0361621-1625, and by the Seventh Framework Programme of the European Commission through grant agreement no. 285939 FP7-REGPOT-2011-1 (ACROSS).

References

[1] Ishikawa J, Furuta K 2006 *Anti-personnel Landmine Detection for Humanitarian Demining* (London: Springer-Verlag London Limited)
[2] Bruschini C 2006 *A Multidisciplinary Analysis of Frequency Domain Metal Detectors for Humanitarian Demining* (PhD Thesis: Vrije Universiteit Brussel)
[3] Das Y 2006 Effects of Soil Electromagnetic Properties on Metal Detector *IEEE Trans. Geosci. Rem. Sens.* **44** 6 1444–1453
[4] Druyts P, Das Y, Craeye C, Acheroy M 2009 Modelling the Response of Electromagnetic Induction Sensors to Inhomogenous Magnetic Soils With Arbitrary Relief *IEEE Trans. Geosci. Rem. Sens.* **47** 8 2627-2638
[5] Dodd C V, Deeds W E 1968 Analytical Solutions to Eddy-current Probe-coil Problems *J. Appl. Phys.* **39** 6 2829–2838
[6] Theodoulidis T P, Kriezis E 2005 Series Expansions in Eddy Current Nondestructive Evaluation Models, *J. Mater. Process. Technol.* **161** 343–347
[7] Silvester P P, Omeragić Dž 1996 Sensitivity Maps for Metal Detector Design, *IEEE Trans. Geosci. Rem. Sens.* **34** 3 788–792